Research Article | Vol. 27, No. 5 | 4 Mar 2019 | OPTICS EXPRESS 7762
Optics EXPRESS

Numerical investigation of imaging-free terahertz generation setup using segmented tilted-pulse-front excitation

GYÖRGY TÓTH,[1,*] LÁSZLÓ PÁLFALVI,[1] JÓZSEF A. FÜLÖP,[2,3,4] GERGŐ KRIZSÁN,[1,3] NICHOLAS H. MATLIS,[5] GÁBOR ALMÁSI,[1,3] AND JÁNOS HEBLING[1,2,3]

[1]*Institute of Physics, University of Pécs, Ifjúság ú. 6, Pécs 7624, Hungary*
[2]*MTA-PTE High-Field Terahertz Research Group, Ifjúság ú. 6, Pécs 7624, Hungary*
[3]*Szentágothai Research Centre, University of Pécs, Ifjúság ú. 20, Pécs 7624, Hungary*
[4]*ELI-ALPS, ELI-Hu Nonprofit Ltd., Dugonics tére 13, Szeged 6720, Hungary*
[5]*Center for Free-Electron Laser Science, Deutsches Elektronen Synchrotron, Notkestrasse 85, Hamburg 22607, Germany*
**tothgy@fizika.ttk.pte.hu*

Abstract: Recently a hybrid-type terahertz (THz) pulse source was proposed for high energy terahertz pulse generation. It is the combination of the conventional tilted-pulse-front setup and a nonlinear crystal with a transmission stair-step echelon of period in the hundred-micrometer range etched into the front face. The tilt angle introduced by the conventional tilted-pulse-front setup (pre-tilt) was chosen to be equal to the tilt-angle needed inside the nonlinear crystal (62° for lithium niobate (LN)) in order to fulfill velocity-matching. In this case, plane-parallel nonlinear optical crystals can be used. The possibility of using a plane-parallel nonlinear optical crystal for producing good-quality, symmetric THz beams was considered the most important advantage of this setup. In the present paper, a thorough numerical investigation of a modified version of that setup is presented. In the new version, the tilted pulse-front is created by a transmission grating without any imaging optics, and a wedged nonlinear optical crystal with a small wedge angle is supposed. According to a 1D numerical code, significantly higher THz generation efficiency can be achieved with a transmission stair-step echelon-faced nonlinear crystal having a 5 – 15-degree wedge angle than with a plane-parallel one or with the conventional tilted-pulse-front setup. Because of the spatially-dependent group-delay dispersion introduced by the transmission grating, a small wedge in the nonlinear crystal improves the spatial homogeneity of the THz-generation process, resulting in higher efficiencies and better beam profiles. At 100 K temperature, and by using 800 nm pump pulses with 20 mJ pulse energy, 100 fs pulse length and 8 mm beam spot radius, approximately 4.5% conversion efficiency and close to 1 mJ terahertz pulse energy can be reached with the newly-proposed setup.

1. Introduction

The study of dynamics and control of materials in the THz frequency range need THz pulses with peak electric fields on the level of 100 kV/cm [1,2]. New, promising applications of intense THz pulses, such as acceleration of electrons [3–5] and protons [6,7], require THz pulses of even higher field strength. Optical rectification of ultrashort laser pulses in nonlinear materials (NM) can be appropriate for efficient generation of such THz pulses. Using the tilted-pulse-front (TPF) technique [8], velocity matching becomes possible also in those cases, where good nonlinear optical properties of the material are vitiated by a larger terahertz index of refraction than the optical one. Presently, this standard, efficient method is applied for various materials. Lithium niobate (LN), which has an extremely high (168 pm/V [9,10]) effective nonlinear optical coefficient and a terahertz refractive index approximately twice that of the optical

#355861 https://doi.org/10.1364/OE.27.007762
Journal © 2019 Received 20 Dec 2018; revised 14 Jan 2019; accepted 15 Jan 2019; published 1 Mar 2019

Optics EXPRESS

refractive index, is suitable for producing THz pulses with mJ-level energy [11] using 800 nm or 1 µm pump wavelengths. Recent results show that semiconductors, such as ZnTe [12] or GaP [13], can also be applied for efficient THz generation if longer pump wavelengths are used to reduce low-order multiphoton absorption. For such long-wavelength pumping, the optical index is significantly smaller than the THz index, necessitating a TPF geometry for these cases as well.

In the TPF excitation geometry, the velocity matching reads as [8]

$$v_{p,gr}\cos(\gamma) = v_{THz,ph}, \tag{1}$$

where $v_{p,gr}$ is the group velocity of the pump pulse, $v_{THz,ph}$ is the phase velocity of the THz pulse, and γ is the pulse-front-tilt angle. The approximate values of γ are 63° for LN at room temperature and 62° at low temperature, respectively, for near infrared pump wavelengths. The highest THz pulse energies in the 0.2 to 1.0 THz range [11] – which are most useful for particle acceleration – have been produced in LN-based TPF setups.

Using LN with the TPF technique has proven very effective and thus has been widely applied. However, the large tilt-angle required and the correspondingly large angular dispersion of the pump beam can severely limit efficient generation of high energy THz pulses with good beam quality. Imaging errors in the presence of angular dispersion result in a lengthened pulse duration at the edges of the pump spot [14,15]. In order to enable perpendicular incoupling of the pump and perpendicular outcoupling of the THz beam, a prism-shaped nonlinear crystal must be used with a wedge angle equal to the required tilt angle γ. The use of a prism results in THz pulses with temporal profiles that vary spatially within the beam due to the variation in interaction length. The results are poor quality, strongly asymmetric THz beams that drastically hinder many applications, especially particle acceleration. In principle, both of these problems can be eliminated by using a contact-grating setup [16] in which the diffraction from an optical grating created directly in the input surface of the NM introduces the TPF of the pump pulse. An efficient contact-grating set-up was realized using ZnTe semiconductor as nonlinear material [12]. Contact grating setups were also designed and realized for LN [17,18]. However, because of technical difficulties induced by the large tilt angle required for LN, efficient THz pulses generation has not yet succeeded.

A third limiting effect of the large tilt angle and the correspondingly large angular dispersion is caused directly by the associated large group-delay-dispersion (GDD) [19]. Because of the large GDD, the temporal intensity profile of an ultrashort pump pulse evolves very fast inside the LN crystal. As a result, the average pump-pulse duration is much longer than the transform limited one, and the average intensity is much lower than the peak. In order to mitigate this problem, a modified version of the tilted-pulse-front THz generation was introduced [20]. In this setup, a discrete TPF is formed by reflecting the pump beam on a stair-step echelon, and this segmented intensity front generates the THz pulse inside the NM. Efficient generation of THz pulses by 70 fs long pump pulses was demonstrated [20]. Disadvantageously, however, this echelon setup also requires a prism-shaped NM with the same large wedge angle, γ, as the conventional setup.

Recently a new hybrid-type setup, a so called “nonlinear echelon slab” (NLES) was proposed [21], which is a combination of the conventional TPF scheme, containing diffraction optics and imaging, and a NM with an echelon-like profile created on its entrance surface. Since the total pulse front tilt is produced in two steps: pre-tilt by the conventional TPF setup and the tilt caused by the entrance surface of the NLES, a beam with reduced angular dispersion falls on the lens resulting in reduced imaging errors. It has been shown that contrary to all the setups used so far, a plane-parallel nonlinear crystal can be used if the pre-tilt angle is equal to the tilt angle inside the NM needed for velocity-matching according to Eq. (1) (62° for the case of LN and low temperature) [21]. Hence the absorption, and dispersion are uniform across the output THz beam profile. This advantage, together with the reduced imaging errors, may lead to the realization of a scalable THz pulse source with good output beam quality (i. e. symmetric beam

Optics EXPRESS

profile) for applications. Very recently a successful proof of principle experiment with such NLES setup was performed [22].

In the present paper we thoroughly investigate with numerical simulations a simplified version of the NLES setup introduced in [21]. Our investigation is not restricted to the case of plane-parallel NLES. We vary the pre-tilt angle in the range of 0° to 76.7° and choose the wedge angle of the NLES so that the velocity matching is fulfilled and the generated THz pulse propagates perpendicularly to the output surface of the NLES. Instead of an optical grating – imaging system, only a transmission grating is used for creating the pre-tilt of the pump intensity front, since such a system is simpler, and scaling it to high pulse energies is more straightforward.

2. Description of the investigated NLES based hybrid setup

The NLES-based hybrid setup considered here consists of only an optical transmission grating and a NLES, as shown in Fig. 1. The echelon slab is made of the material of the nonlinear crystal itself (LN is supposed), and has a period in the hundred-micron range. Contrary to the case in [21], our investigation now is not restricted to a plane-parallel NLES. Instead, the γ_0 pre-tilt introduced by the transmission grating (TG) is varied between 0° and 76.7°, and the γ_{slab} tilt angle of the NLES, and the δ_w wedge angle of the NLES are chosen such that two conditions will be satisfied for each given γ_0. First, the velocity matching condition according to Eq. (1) must be fulfilled. This requires:

$$\tan(\gamma_{slab}) = \frac{h}{w} = \frac{n_{p,gr}\tan(\gamma) - \tan(\gamma_0)}{n_{p,gr} - 1}, \tag{2}$$

where $n_{p,gr}$ is the pump group index of refraction. Second, the output surface of the NLES is set to be perpendicular to the propagation direction of the generated THz pulse, requiring

$$\delta_w = \gamma - \gamma_{slab} \tag{3}$$

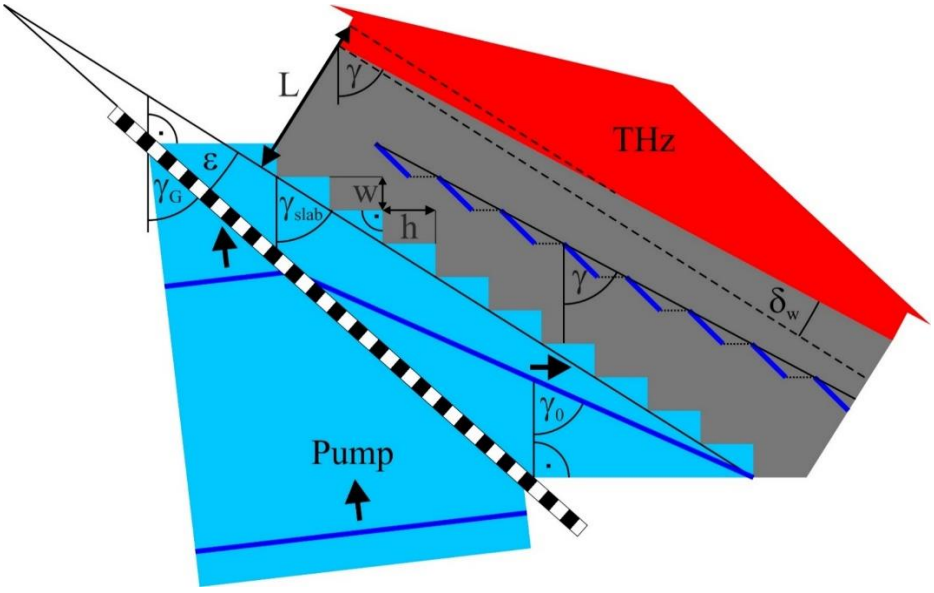

Fig. 1. The setup of the investigated hybrid NLES THz source. The dark blue lines represent the pump pulse front at different moments. After diffraction of the pump beam on the transmission grating (TG), it propagates horizontally. Consequently, the phase-fronts are vertical. All γ is measured from a vertical line.

Optics EXPRESS

For the extreme case of $\gamma_0 = 0°$ the setup consists of only an appropriate NLES, but does not contain a TG. For $\gamma_0 = 62°$ a plan-parallel NLES can be used and the setup become similar to the one investigated in [21], with the only difference that now the setup does not consist of imaging, just a TG is used for introducing the pre-tilt. For the other extreme case of $\gamma_0 = 76.7°$ the setup becomes very similar to the conventional TPF setup, with the only difference that now the setup does not consist of imaging. (Entering perpendicular a beam with $\gamma_0 = 76.7°$ tilt angle into the LN prism, the tilt angle will be reduced inside the LN to $\gamma = 62°$).

Figure 2(a) and 2(b) show the dependence of the γ_{slab} tilt angle and the δ_w wedge angle of the NLES, and the ε angle between the plane of the TG and the plane of the average input surface of the NLES on the γ_0 pre-tilt angle for 800 nm and 1030 nm pump wavelengths. Here it was supposed that the TG is used in Littrow arrangement, which results in the largest diffraction efficiency.

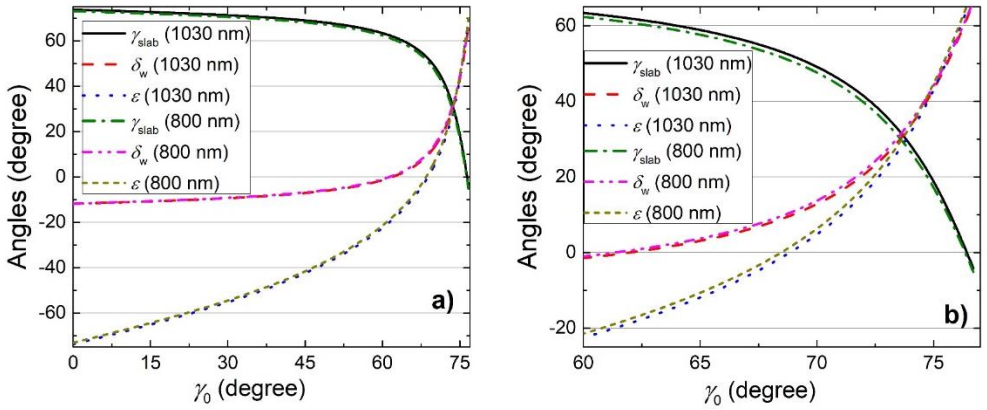

Fig. 2. (a) The dependence of the γ_{slab} tilt angle and of the δ_w wedge angle of the NLES, and the ε angle between the plane of the TG and the plane of the average input surface of the NLES on the γ_0 pre-tilt angle. (b) The most important range of (a) on an expanded scale. The temperature was supposed to be 100 K.

According to Fig. 2, in agreement with [21], plan-parallel NLES can be used for $\gamma_0 = 62°$ pre-tilt angle. Furthermore, the δ_w wedge angle remains bellow +/– 16° on the 0° – 71° pre-tilt angle range.

3. Effect of the spatially varying pump chirp

In Section 4 the details of the theoretical model of the THz generation in the NLES will be given. Generally, in TPF-based THz excitation setups, the characteristics of the pump pulse length variation due to material and angular dispersion are key factors from the point of view of the evolution of the THz field. In this section we discuss the effect of the spatially varying pump chirp.

Results of earlier optimization [14,23] show that using pre-chirp in the pump beam leads to enhancement of the THz generation efficiency. Therefore, we assume that the pump beam has an initial chirp when it reaches the TG. The diffraction from the TG introduces an angular dispersion on the pump beam that is modified when the pump enters into the NLES due to refraction and material dispersion. The spatial variation of the pump pulse length due to the dispersion must be considered in our special case when the evolution of the THz field is described. Let see Fig. 3(a) for the determination of the $\tau(z')$ local pump pulse length along the THz propagation path. The pump pulse arriving at C can be characterized by a parameter, $\Delta\tau_0$, which is the group delay difference between the short and long wavelength components resulting from the initial chirp and the group delay difference accumulated along AC. One must pay attention to the noncollinear propagation and the spatial extension of the pump beam: at G (with corresponding z' coordinate in the THz propagation direction) the THz field interacts with

Optics EXPRESS

pump pulse coming from D. Therefore, in accordance with [19] the group delay difference, $\Delta\tau(z')$, at z' (G) can be given as

$$\Delta\tau(z') = \Delta\tau_0 + \frac{\lambda_0}{c}(DF - AC)\left[\frac{\tan(\gamma_0)}{\lambda_0}\right]^2 \Delta\lambda + \frac{\lambda_0}{c} FG\left\{n_{p,ph}\left[\frac{\tan(\gamma_0)}{n_{p,ph}\lambda_0}\right] - \frac{d^2 n_{p,ph}}{d\lambda^2}\right\}\Delta\lambda, \quad (4)$$

where λ_0 is the central wavelength of the pump, $\Delta\lambda$ is the spectral bandwidth (FWHM), $n_{p,ph}$ is the phase refractive index at the pump wavelength. Based on simple geometrical considerations (Fig. 3(a)), it can be seen that

$$DF - AC = z'\sin(\gamma)\left[\tan(\gamma_G) - \tan(\gamma_{slab})\right], \quad (5)$$

and

$$FG = z'\left[\cos(\gamma) + \sin(\gamma)\tan(\gamma_{slab})\right]. \quad (6)$$

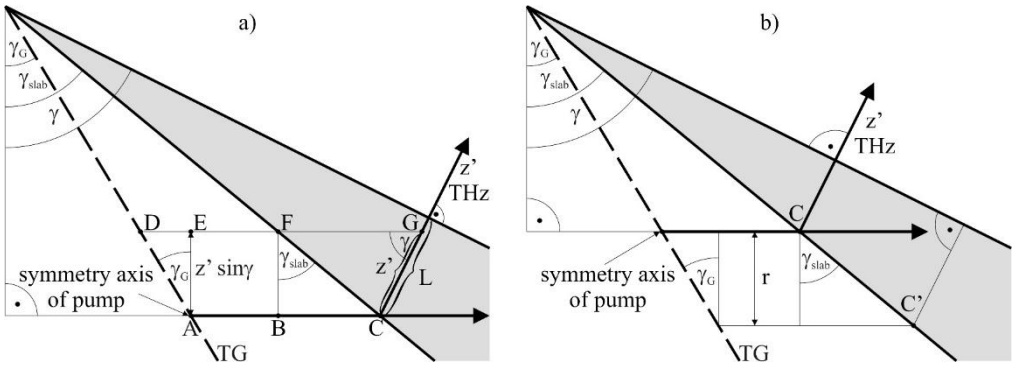

Fig. 3. Illustration for the determination of the local pump pulse length (a) along the center of the THz beam (z') and (b) along an axis parallel with z' at a distance of r_{NM} in the lateral plane.

The discussion of the non-uniformity of the generated THz beam is an essential part of the present paper. Therefore, it is important to describe the local pump pulse length in the lateral plane along an axis parallel to the z' axis (symmetry axis of the THz beam) at a distance of r_{NM} as well (see Fig. 3(b)). In this case, Eqs. (4)-(6) can be also used, but according to Fig. 3(b) in Eq. (4) $\Delta\tau_{C'}$ has to be written instead of $\Delta\tau_0$, where

$$\Delta\tau_{C'} = \Delta\tau_0 + \frac{\lambda_0}{c} r\left[\tan(\gamma_{slab}) - \tan(\gamma_G)\right]\left(\frac{\tan(\gamma_0)}{\lambda_0}\right)^2 \Delta\lambda. \quad (7)$$

Furthermore, one has to take into account, that the THz propagation path is $L + r_{NM}\tan(\delta_w)$ according to Figs. 3(a) and 3(b).

4. Description of the numerical model

A simple model was developed in order to obtain quantitative information on the optical-to-THz conversion efficiency and on the THz waveform and spectra for the NLES setup introduced in Section 2. The model described in [14,21,24] for THz generation by optical rectification was adapted to the proposed new setup by considering the following special effects: (i) the variation of the pump pulse length according to Eqs. (4)-(6), (ii) the variation of the pump intensity due to diffraction, (iii) the dephasing effect on the THz radiation due to the segmented structure of the pump pulse front (as illustrated in Figs. 3 and 5 of [21]).

Let us suppose that the initial temporal shape of the optical pump pulse is $\tilde{E}(t) = E_0 \exp\left[-2\ln(2)t^2/\tau_0^2\right]\exp(i\omega_0 t)$, where E_0 is the peak electric field-strength and τ_0 is

Optics EXPRESS

the transform-limited (TL) pump pulse length (FWHM). Taking into account the nonlinear polarization in the same way as in [24], the differential equation for the $E_{\mathrm{THz}}(\Omega, z')$ Fourier component of the THz field reads as:

$$\frac{\partial}{\partial z'}E_{\mathrm{THz}}(\Omega,z') = -\mathrm{i}\frac{\Omega d_{\mathrm{eff}}E_0^2\tau_0}{2\sqrt{4\pi\ln(2)}cn_{THz,ph}(\Omega)}\exp\left[-\frac{\left(\tau_0^2+\Delta\tau(z')^2\right)^2\Omega^2}{16\ln(2)}\right]\times \exp\left[\mathrm{i}\frac{\Omega}{c}\left(n_{THz,ph}(\Omega)-\frac{n_{p,gr}}{\cos(\gamma)}\right)z'\right]f(z')g(z')-\frac{\alpha(\Omega)}{2}E_{\mathrm{THz}}(\Omega,z') \quad (8)$$

where c is the speed of light in vacuum, Ω is the angular frequency of the THz radiation, $n_{\mathrm{THz,ph}} = c/v_{\mathrm{THz,ph}}$ is the THz phase index of refraction, $\alpha_{\mathrm{THz}}(\Omega)$ is the THz (intensity) absorption coefficient, d_{eff} is the effective nonlinear coefficient ($d_{\mathrm{eff}} = d_{33} = 168$ pm/V for LN), and $n_{\mathrm{p,gr}}$ is the group refractive index of the pump. The meaning of f(z') and g(z') factors will be given afterwards.

As mentioned above, one way to increase the effective interaction length (defined in [14]) is to compensate for the effects of material and angular dispersion (see the second term of Eq. (2)), by pre-chirping the pulses [14,23]. In this way, one can set the pump-pulse length to be minimal (i.e., equal to the TL value) not at the entrance, but inside the crystal by tuning the $\Delta\tau_0$ parameter. Instead of following the complex optimization procedure given in [23], we set the TL pulse length value at the crystal center (at $z' = L/2$, where L is the length of the slab along the z' axis as shown in Fig. 3(a)) [14]. In this way, a significant efficiency enhancement can be achieved keeping the calculations simple. Numerical simulations were performed under this condition, and the results are shown in the next section.

Due to the diffraction of the pump beam, the w' width of one segment of the pulse front increases with the pump propagation coordinate, z_p (i.e., the distance FG in Fig. 3(a)) and consequently with z' as well. The relation between z_p and z' is $z_p = z'[\cos(\gamma) + \sin(\gamma)\tan(\gamma_{\mathrm{slab}})]$, which is used in Eqs. (9) and (10). Assuming a simple linear dependence of w' on z':

$$w'(z') = w+\frac{z_p\lambda_0}{wn_{p,ph}} = w+\frac{z'\lambda_0}{wn_{p,ph}}\left[\cos(\gamma)+\sin(\gamma)\tan(\gamma_{slab})\right]. \quad (9)$$

On the one hand, as a consequence of the pump diffraction the pump intensity decreases. On the other hand, the THz energy is proportional to the area of the pump segment as well. These effects can be taken into consideration with the following propagation dependent factor:

$$f(z') = \frac{1}{\sqrt{1+\frac{z_p\lambda_0}{w^2n_{p,ph}}}} = \frac{1}{\sqrt{1+\frac{z'\lambda_0}{w^2n_{p,ph}}\left[\cos(\gamma)+\sin(\gamma)\tan(\gamma_{slab})\right]}}. \quad (10)$$

The THz wavelets originating from the different points of the segmented pump pulse front experience a periodically varying phase shift due to the differences in the propagation paths to a far plane. In order to describe the influence of this effect on the THz generation efficiency, it is useful to introduce, as in [21], the factor

$$g(z') = \sin c\left[\pi x'(z')\right], \quad (11)$$

where x = m'/λ', and $m'(z') = w'(z')\left[\tan(\gamma)-\frac{\tan(\gamma_0)}{n_{\mathrm{p,gr}}}\right]\cos(\gamma)$.

The second exponential factor in Eq. (8) takes into account any remaining mismatch of the noncollinear velocity-matching setup. Terahertz absorption, which is taken into account in the

Optics EXPRESS

very last term of Eq. (8), is related only to the lattice. Absorption by free-carriers, generated by multiphoton absorption is neglected. Any other effects, such as pump depletion, and self-phase modulation were also neglected.

The THz fluence at the output can be determined from the solution of Eq. (8) as

$$Fluence_{THz} = \frac{\varepsilon_0 c}{2} 2\pi \int_0^\infty \left| E_{THz}(\Omega, L) \frac{2n_{THz,ph}}{n_{THz,ph}+1} \right|^2 \mathrm{d}\Omega. \tag{12}$$

Fresnel reflections, which cause a significant loss, is also accounted for in this formula. The pump fluence is:

$$Fluence_p = \sqrt{\frac{\pi}{2}} \frac{c\varepsilon_0 n_{p,ph}}{2} E_0^2 \frac{\tau_0}{\sqrt{2\ln(2)}} \tag{13}$$

and the optical-to-THz conversion efficiency is thus:

$$\eta = \frac{Fluence_{THz}}{Fluence_p}. \tag{14}$$

Here we briefly summarize the differences between the models used here and in [21]. (i) Since in present work no imaging was applied, the spatial behavior of the pump pulse length is different. (ii) the factor f(z') (Eq. (10)) which is responsible for the variation of the pump intensity differs from the one given in [21]. The reason is that by mistake in [21] it was not taken into consideration that the THz energy is proportional to the area of the pump segment as well. (iii) Contrary to [20] we find it unnecessary to attribute any effect to the "duty cycle" (defined by Eqs. (11) and (12) in [21]) related to the periodic discontinuity of the pump pulse front. Since then we have understood that since the whole pump power is presented only in a smaller area (and consequently with higher pump intensity), the THz conversion efficiency remains independent from the "duty cycle". (iv) Based on recent investigations, it was found that using 30 fs long pulses, the damage threshold intensity is ~1 TW/cm^2 [25], and the damage threshold of crystals is approximately proportional to $1/\sqrt{\tau_0}$ [26]. Therefore, instead of using constant intensity as in [21], the pump intensity was chosen according to $=100\frac{\mathrm{GW}}{\mathrm{cm}^2}\sqrt{\frac{100\,\mathrm{fs}}{\tau_0}}$, which keeps it about five times below the damage threshold for any supposed τ_0 values.

5. Results and discussion

The shape of the generated terahertz pulses and the generation efficiency depend on many parameters. Therefore, for presenting the results the following strategy was chosen: i) First the dependence of the efficiency on the phase matching frequency and the w step width of the echelon structure of the NLES were investigated for a few pre-tilt angles. Then, the find optimal step width and phase matching frequency were chosen in later calculations. ii) The dependence of the generation efficiency on the crystal length in different pre-tilt cases was investigated. iii) Finally, the waveform of the generated THz pulse was presented and comparison with the conventional prism-based setup was done.

5.1. Efficiency curves

First a pump intensity of 100 GW/cm^2 and a pump wavelength of 800 nm, and pump pulse duration of 100 fs were assumed. Note that the results are very similar to the case of a 1030 nm pump wavelength.

Figure 4(a) shows the dependence of efficiency on the phase matching frequency and on the step width at 100 K temperature and 68° pre-tilt angle. The THz generation is most efficient

Optics EXPRESS

for phase-matching frequencies in the 0.6 - 1.0 THz range and step widths in the 60 - 80 µm range. It is well known that the generation efficiency is proportional to the square of the phase-matching frequency [24], but THz absorption in LN crystals are also larger at for higher frequencies. Consequently, the most efficient THz generation is achieved at a relatively low frequency. Regarding the dependence of the efficiency on the step width, it can be said that a narrower step width causes larger pump diffraction and consequently more rapid decrease of the pump intensity inside the crystal, leading to the reduction of the THz-generation efficiency. On the other hand, for larger step widths, the significance of the de-phasing effect described by Eq. (11) increases, leading to the reduction of the efficiency. Therefore, the most efficient THz generation is achieved for step widths in the range of 60 - 80 µm.

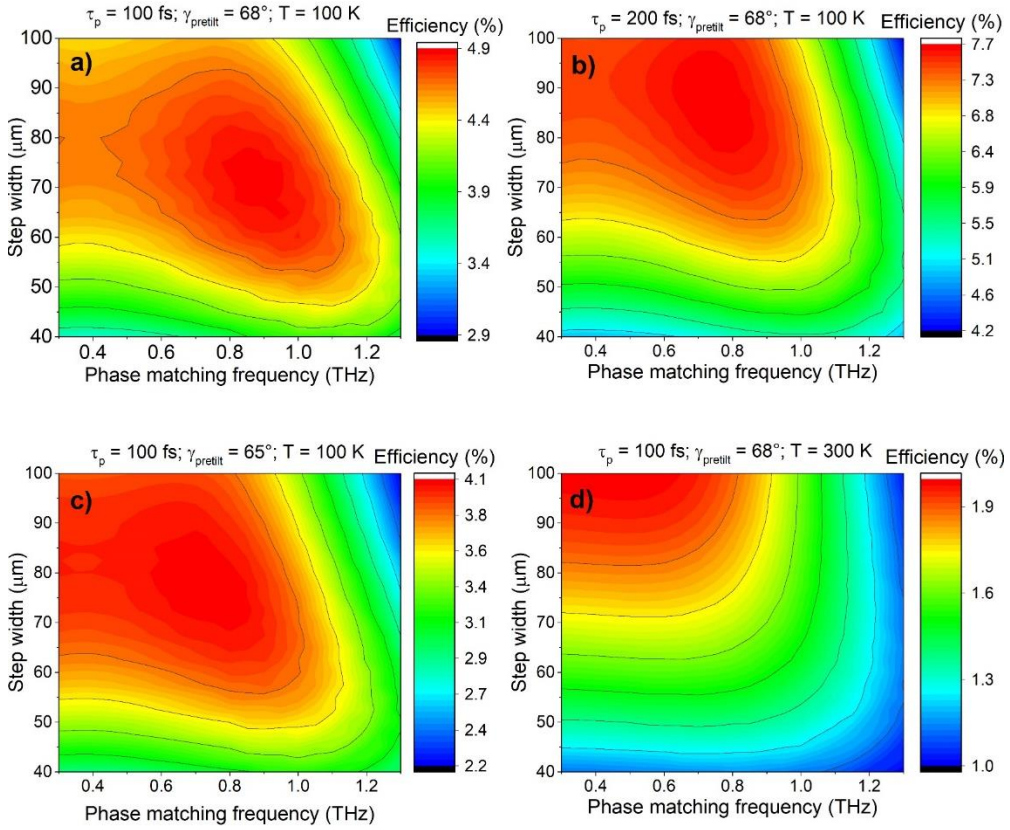

Fig. 4. The efficiency versus the step width and the phase matching frequency for four different cases. The values of pump pulse duration, pre-tilt angle, and temperature are indicated on the top of the contour plots.

Using longer pump pulse durations, larger THz generation efficiencies can be achieved, as shown in Fig. 4(b). The reason of this is that the pump pulse duration does not change as fast as in case of shorter pulses, and therefore the intensity is on average higher during the THz-generation process. Similarly, one might expect increasing efficiencies for decreasing pre-tilt angles, since the angular dispersion is smaller. However, since the above-mentioned de-phasing effect is smaller for larger pre-tilt angles, the net effect is for efficiencies to be larger for larger pre-tilt angles (Fig. 4(a)) than for lower pre-tilt angles (Fig. 4(c)).

As expected, because of the increased THz absorption, at room temperature (Fig. 4(d)) the highest efficiency is more than two times smaller than at low temperature (Fig. 4(c)). Furthermore, at room temperature the highest efficiency belongs to a step width of ~100 µm.

Optics EXPRESS

However, to utilize the advantage of the large step widths (and reduced diffraction), impractically-long crystals are needed and the frequency of the generated THz pulse becomes low.

According to Figs. 4(a)-4(c), w = 70 μm and ν_0 = 0.8 THz are close to the optimal choice at 100 K. In the remaining part of this paper, calculation results obtained for these parameters will be presented.

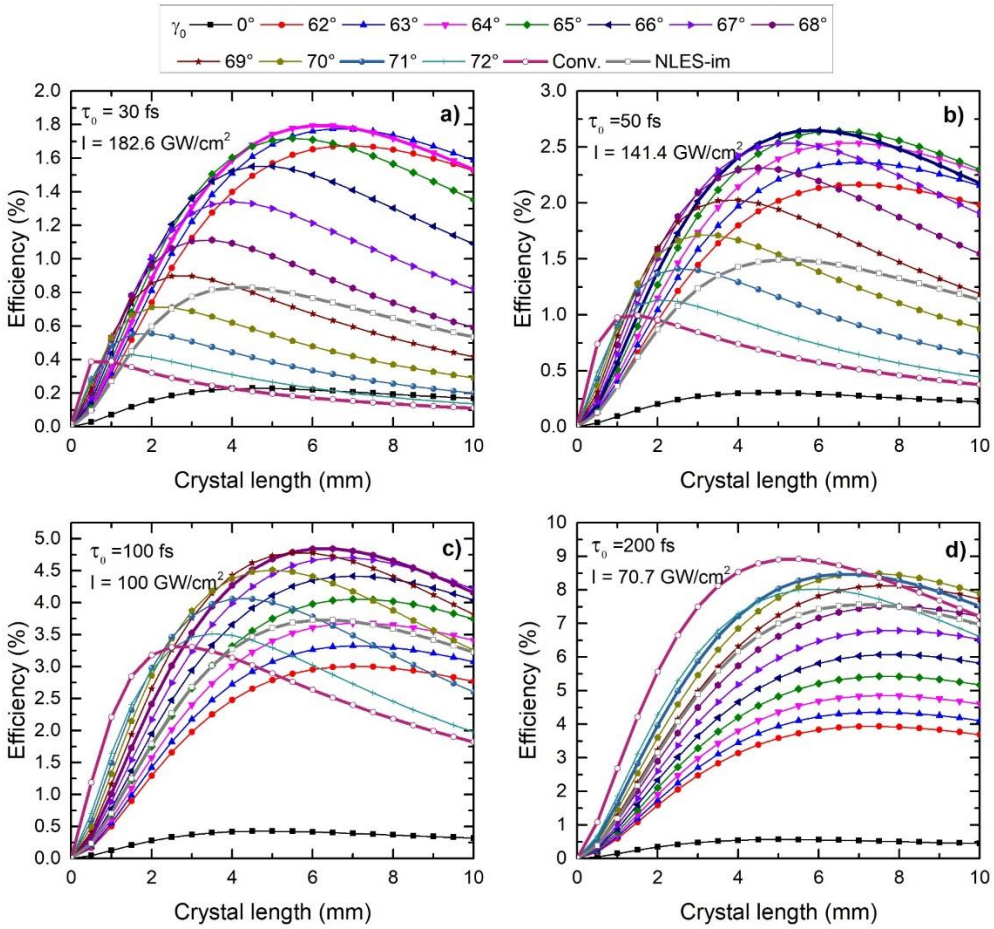

Fig. 5. THz generation efficiency curves plotted versus the crystal length for certain pre-tilt angles and for the conventional setup as well. The pump wavelength was 800 nm and the temperature was 100 K in all cases. The pulse durations and the intensities are indicated in the Figs.

In order to determine the optimal pre-tilt angle, the THz-generation efficiency dependence on the crystal length was investigated in case of different pre-tilt angles and pump-pulse durations. The results of these calculations are shown in Fig. 5. For the sake of comparison, the Fig. also shows the efficiencies belonging to the conventional, prism-based THz sources (labeled as 'Conv.' in Fig. 5). An important difference between the conventional and the currently-introduced NLES is that the conventional setup requires imaging optics and the new one doesn't. Consequently, effects of imaging errors [27] are eliminated. In addition, the lower angular dispersion required in the new setup results in less pump-pulse broadening and therefore less reduction in the average compared to the peak intensity. This effect becomes more significant as the pulse duration decreases and the corresponding optical bandwidth increases. Our calculations predict that conversion efficiencies using pulses with shorter than

Optics EXPRESS

200 fs durations are significantly improved using the new setup compared to the conventional one.

Using the NLES setup without imaging thus allows higher energies to be achieved than using NLES with imaging (shown as NLES-im in Fig. 5). For shorter pump pulses, the degree of pump-pulse length variation inside the crystal is the most relevant factor determining the efficiency. For a pre-tilt angle of about 61° in the imaging-free NLES, a special condition is achieved in which there is a nearly constant pump pulse length along the THz propagation (discussed in detail in the next subsection). In contrast, for the NLES that employs imaging, the pump pulse length changes significantly during the nonlinear interaction. Consequently, higher efficiency can be achieved with the imaging-free NLES. For longer pulses, the de-phasing effect coming from the echelon structure has a significant influence on the efficiency. Hence, for larger pre-tilt angles (and consequently lower de-phasing factors) larger efficiencies can be achieved.

Comparing the four plots of Fig. 5, a decreasing optimal pre-tilt angle with decreasing pump pulse duration can be observed. This can be also explained by the increasing effect of the angular dispersion with decreasing pump pulse duration.

Our calculations show that using a pumping wavelength of 1030 nm, the achievable efficiency is only 75% of the efficiency at 800 nm wavelength. The reason for this decrease is that for longer pumping wavelength, the effect of diffraction on the pump beam segments resulting from the stair-steps of the echelon is more significant than for shorter pumping wavelengths. As a consequence, at 1030 nm pumping, the intensity of the segments decreases more rapidly than in the case of 800 nm pumping. For longer pumping wavelengths, the efficiency curves reach their maximum at about 20% shorter crystal lengths.

At room temperature, depending on the pre-tilt angle, the pump-pulse duration and the pump wavelength, the maximum efficiency drops by a factor of 1.7 – 2.6 as compared to the 100 K case. This is due to the significant increase of the THz absorption of the LN crystal at room temperature [28,29].

5.2. The THz waveforms

In the following section, we describe the result of calculations assuming a pump-pulse duration, wavelength, and intensity of 100 fs, 800 nm, and 100 GW/cm^2, respectively. Figure 6 shows the THz waveforms (Figs. 6(a)-6(b) and their spectra (Fig. 6(c)) for four different pre-tilt angles. The waveforms of the pulses are near single-cycle apart from the decaying oscillations at the end of the pulse. These oscillations are more significant for higher pre-tilt angles. The most intensive pulse belongs to the 68° pre-tilt angle case. The calculations show that the larger a pre-tilt is used, the more the central frequency of the spectrum shifts towards higher frequencies (see in Fig. 6(c)). There are several reasons for this effect: on the one hand, in the case of larger pre-tilt angles, the de-phasing described by Eq. (11) is smaller, and thus the THz spectra are shifted to higher frequencies. On the other hand, for larger pre-tilt angles, shorter crystal lengths are required to achieve the highest efficiency. However, for shorter crystal lengths, there is less THz absorption within the crystal. Since the THz absorption is a monotonically increasing function of frequency [28,29], reducing absorption effectively shifts the spectrum towards higher frequencies.

Optics EXPRESS

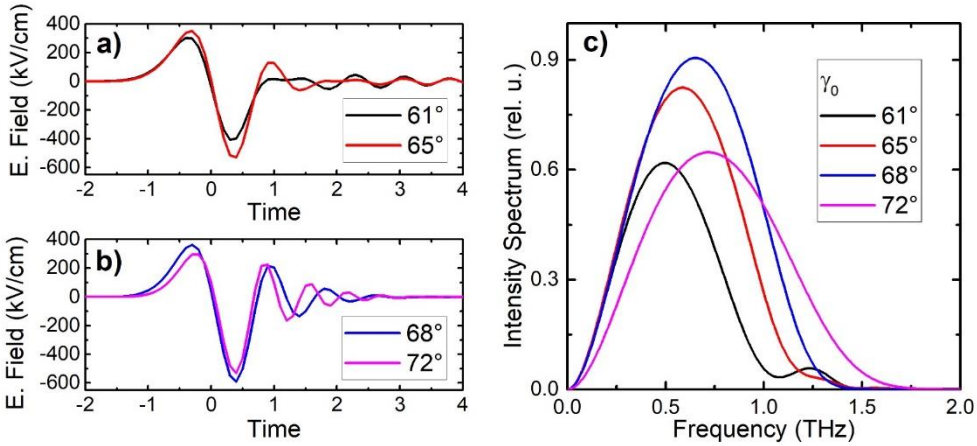

Fig. 6. Waveforms of the generated THz pulse for four different pre-tilt angles (a, b) and their spectra (c).

Figure 7 shows the THz waveforms belonging to three points chosen symmetrically along the beam cross section (r = 0 and ± 4 mm, for illustration see Fig. 3(b)).

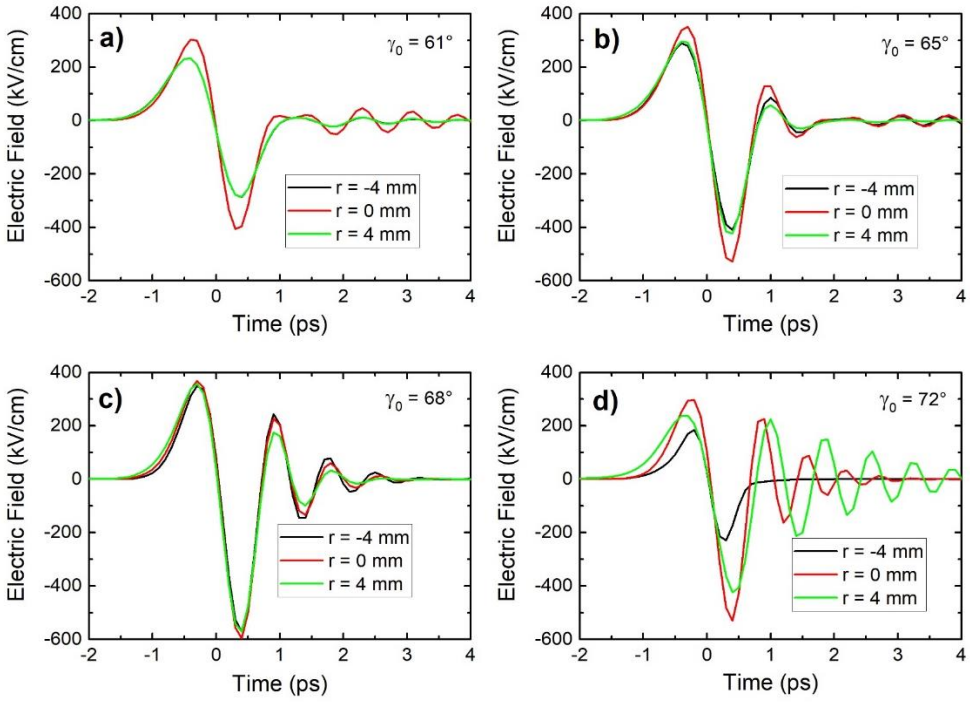

Fig. 7. Waveforms of the THz pulses generated by the NLES setup. The three curves on every graph belong to three different points on the beam cross section. 800 nm wavelength, 100 fs pump pulse length and 100 K temperature were assumed. The pre-tilt angles are (a) 61° (b) 65° (c) 68° and (d) 72°, respectively.

In order to understand the formation of different pulse shapes, it is essential to monitor the variation of the pump pulse length during the THz generation process according to Eq. (7). For THz waveforms shown in Fig. 7(a)-7(d), Fig. 8(a)-8(d) show the corresponding pump pulse lengths along the propagation of the given THz wavelet.

Optics EXPRESS

Figure 8(a) shows the special case for which the pulse length within the crystal essentially does not change along the THz generation path. Since the pre-chirp was set so as to ensure a Fourier-limited pulse length value at r = 0 and z' = L/2, the pulse will be Fourier-limited along the whole path along z'. By moving symmetrically from r = 0, oppositely chirped pulses will enter into the crystal. The structure is nearly planar for the 61° pre-tilt, so that the propagation paths of the THz wavelets along the beam cross section are independent of *r*. As a consequence, a THz beam is generated whose frequency decreases with the distance from the beam center (r = 0).

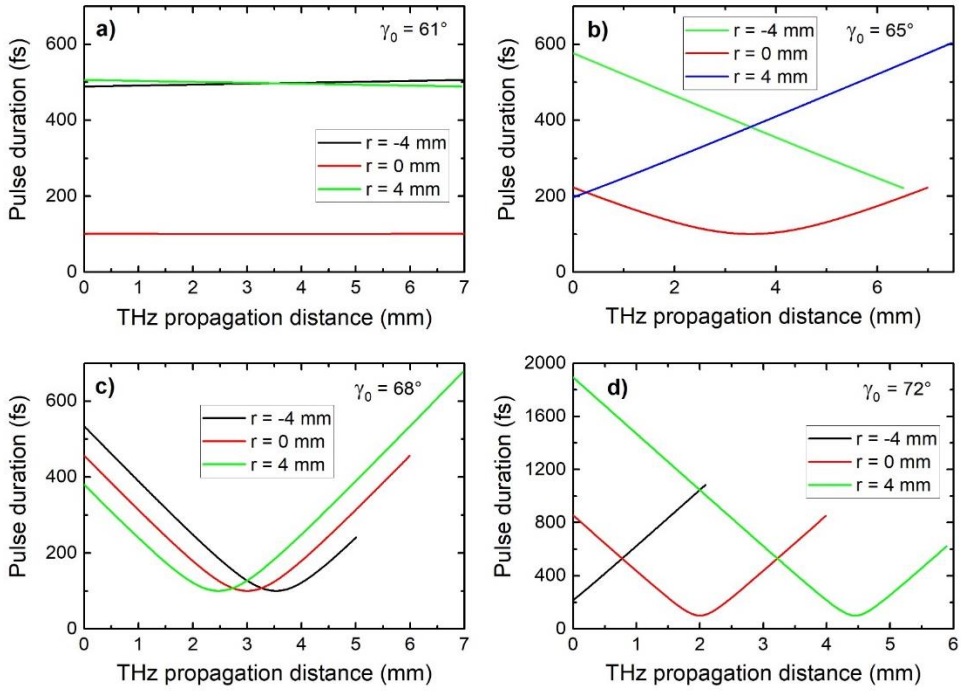

Fig. 8. Variation of the pump pulse length along the propagation of the given THz wavelet. All parameters are identical to those of Fig. 7.

Increasing the angle of the pre-tilt (Figs. 7(b)-7(d)), we find that in the case of 68°, the shape of the THz pulse does not change significantly along the cross-section of the beam (Fig. 7(c)). This is due to the fact that the spatial averages of the pulse lengths along the THz generation path are nearly equal (see the three curves in Fig. 8(c)). We can conclude, that (in contrary to a naïve guess), the most homogeneous generation of high energy THz pulses are possible by using not a plan-parallel NLES, but instead by using a wedged NLES with δ_w = 8.62° (corresponding to 68° pre-tilt angle). The reason is that the pump pulse evolves not only inside the NLES, but in the space between the TG and the NLES as well. It is worth to note that in the setup using imaging of the TG (as was supposed in [21]), plane-parallel NLES generates the most homogeneous THz pulses.

Figure 9 shows the advantage of our setup compared to the conventional prism-based imaging case. Figure 9(a) shows a 2D contour plot of the shape of the generated THz pulse along the transversal dimension using NLES with a 68° pre-tilt angle. For transparency, three cuts were done from this Fig. and plotted in Fig. 9(b). Figures 9(c) and 9(d) show the THz-pulse generated by the conventional setup. In both cases, the length of the crystal at the center of the THz beam cross section was assumed to be equal with the length resulting in the highest efficiency according to the previous calculations (see in Fig. 5(c)). The crystal lengths were thus 6.5 mm and 2.5 mm for the new NLES setup and the conventional setup, respectively.

Optics EXPRESS

Under these circumstances, the transverse extent of the crystal is restricted to the r > –2.8 mm region for the conventional setup.

Using NLES (Fig. 9(a)-9(b)), the THz waveform is almost uniform along the transversal dimension (*r*) contrary to the conventional prism-based setup (Fig. 9(c)-9(d)). While for the NLES setup, the pulse shape remains nearly single-cycle along the entire range of *r* contrary to this for the conventional setup the number of the cycles increase with *r*. Besides, the wavefronts are parallel for the NLES but curved for the conventional setup. So it can be clearly seen that the NLES-based THz pulse source provides significantly better THz beam and pulse quality for high intensity THz applications than the conventional setup.

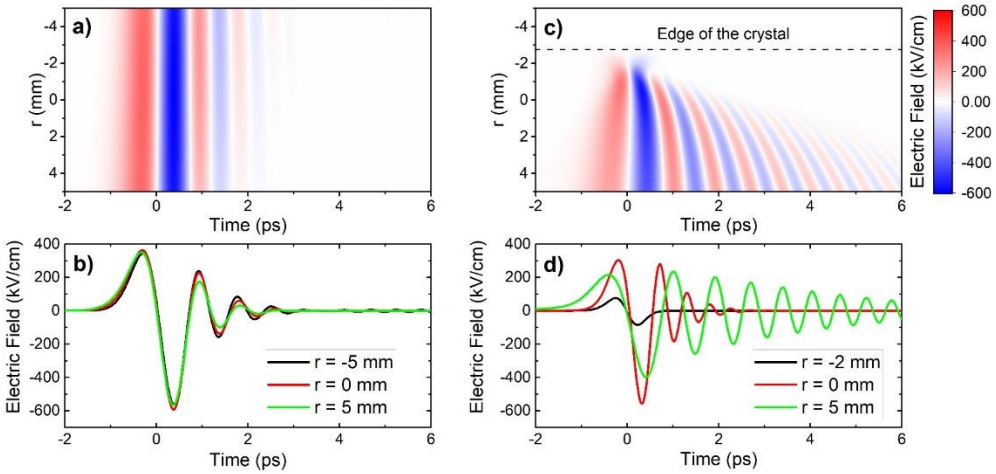

Fig. 9. Pulse shape of the generated THz pulse using the NLES setup (a)-(b) and the conventional tilting pulse front based setup (c)-(d).

6. Conclusions

An NLES-based, energy-scalable, compact THz pulse source was introduced. Its significant advantage compared to the prism-based conventional tilted-pulse-front setup is that imaging optics can be omitted, allowing imaging errors to be avoided. A theoretical model was developed to examine the optical-to-terahertz conversion efficiency and the THz pulse-shape characteristics. It was shown, that using pump pulses shorter than 200 fs, significantly higher optical-to-THz conversion efficiencies can be achieved than with the conventional setup. For example, with a 50 fs pump pulse, a 2.5-fold efficiency enhancement can be achieved. Moreover it was shown, that a special geometry can be found (by setting the pre-tilt angle to 68°, and the wedge angle to 8.62°) with which uniform THz waveform can be achieved along the whole beam cross section, making possible several applications and perfect focusing.

Present calculations are limited to using the transmission grating in Littrow-configuration. Studying the possibilities of detuning the setup configuration from the Littrow is the subject of a future investigation.

Funding

Nemzeti Kutatási, Fejlesztési és Innovációs Hivatal (NKFIH) (125808; 2018-1.2.1-NKP-2018-00010, financed under the 2018-1.2.1-NKP funding scheme); ÚNKP-17-3-I New National Excellence Program of the Emberi Eroforrások Minisztériuma, European Union, co-financed by the European Social Fund grant EFOP-3.6.1.-16-2016-00004 entitled by Comprehensive Development for Implementing Smart Specialization Strategies at the University of Pécs and grant EFOP-3.6.2-16-2017-00005 entitled by Ultrafast physical processes in atoms, molecules, nanostructures and biology structures.

Optics EXPRESS

References

1. T. Kapfrath, K. Tanaka, and K. A. Nelson, "Resonant and nonresonant control over matter and light by intense terahertz transients," Nat. Photonics **7**(9), 680–690 (2013).
2. D. Nicoletti and A. Cavalleri, "Nonlinear light–matter interaction at terahertz frequencies," Adv. Opt. Photonics **8**(3), 401 (2016).
3. E. A. Nanni, W. R. Huang, K.-H. Hong, K. Ravi, A. Fallahi, G. Moriena, R. J. Miller, and F. X. Kärtner, "Terahertz-driven linear electron acceleration," Nat. Commun. **6**(1), 8486 (2015).
4. D. Zhang, A. Fallahi, M. Hemmer, X. Wu, M. Fakhari, Y. Hua, H. Cankaya, A.-L. Calendron, L. E. Zapata, N. H. Matlis, and F. X. Kärtner, "Segmented terahertz electron accelerator and manipulator (STEAM)," Nat. Photonics **12**(6), 336–342 (2018).
5. Z. Tibai, M. Unferdorben, S. Turnár, A. Sharma, J. A. Fülöp, G. Almási, and J. Hebling, "Relativistic electron acceleration by focused THz pulses," J. Phys. At. Mol. Opt. Phys. **51**(13), 134004 (2018).
6. L. Pálfalvi, J. A. Fülöp, G. Tóth, and J. Hebling, "Evanescent-wave proton postaccelerator driven by intense THz pulse," Phys. Rev. Accel. Beams **17**, 031301 (2014).
7. A. Sharma, Z. Tibai, and J. Hebling, "Intense tera-hertz laser driven proton acceleration in plasmas," Phys. Plasmas **23**(6), 063111 (2016).
8. J. Hebling, G. Almási, I. Kozma, and J. Kuhl, "Velocity matching by pulse front tilting for large area THz-pulse generation," Opt. Express **10**(21), 1161–1166 (2002).
9. Q. Wu and X. C. Zhang, "Ultrafast electro-optic field sensors," Appl. Phys. Lett. **68**(12), 1604–1606 (1996).
10. J. Hebling, A. G. Stepanov, G. Almási, B. Bartal, and J. Kuhl, "Tunable THz pulse generation by optical rectification of ultrashort laser pulses with tilted pulse fronts," Appl. Phys. B **78**, 593–599 (2004).
11. J. A. Fülöp, Z. Ollmann, C. Lombosi, C. Skrobol, S. Klingebiel, L. Pálfalvi, F. Krausz, S. Karsch, and J. Hebling, "Efficient generation of THz pulses with 0.4 mJ energy," Opt. Express **22**(17), 20155–20163 (2014).
12. J. A. Fülöp, G. Polónyi, B. Monoszlai, G. Andriukaitis, T. Balciunas, A. Pugzlys, G. Arthur, A. Baltuska, and J. Hebling, "Highly efficient scalable monolithic semiconductor terahertz pulse source," Optica **3**(10), 1075–1078 (2016).
13. G. Polónyi, M. I. Mechler, J. Hebling, and J. A. Fülöp, "Prospects of Semiconductor Terahertz Pulse Sources," IEEE J. Sel. Top. Quantum Electron. **23**(4), 1–8 (2017).
14. J. A. Fülöp, L. Pálfalvi, G. Almási, and J. Hebling, "Design of high-energy terahertz sources based on optical rectification," Opt. Express **18**(12), 12311–12327 (2010).
15. M. Kunitski, M. Richter, M. D. Thomson, A. Vredenborg, J. Wu, T. Jahnke, M. Schöffler, H. Schmidt-Böcking, H. G. Roskos, and R. Dörner, "Optimization of single-cycle terahertz generation in $LiNbO_3$ for sub-50 femtosecond pump pulses," Opt. Express **21**(6), 6826–6836 (2013).
16. L. Pálfalvi, J. A. Fülöp, G. Almási, and J. Hebling, "Novel setups for extremely high power single-cycle terahertz pulse generation by optical rectification," Appl. Phys. Lett. **92**(17), 171107 (2008).
17. Z. Ollmann, J. Hebling, and G. Almási, "Design of a contact grating setup for mJ-energy THz pulse generation by optical rectification," Appl. Phys. B **108**(4), 821–826 (2012).
18. M. Tsubouchi, K. Nagashima, F. Yoshida, Y. Ochi, and M. Maruyama, "Contact grating device with Fabry-Perot resonator for effective terahertz light generation," Opt. Lett. **39**(18), 5439–5442 (2014).
19. J. Hebling, "Derivation of the pulse front tilt caused by angular dispersion," Opt. Quantum Electron. **28**(12), 1759–1763 (1996).
20. B. K. Ofori-Okai, P. Sivarajah, W. Ronny Huang, and K. A. Nelson, "THz generation using a reflective stair-step echelon," Opt. Express **24**(5), 5057–5068 (2016).
21. L. Pálfalvi, G. Tóth, L. Tokodi, Z. Márton, J. A. Fülöp, G. Almási, and J. Hebling, "Numerical investigation of a scalable setup for efficient terahertz generation using a segmented tilted-pulse-front excitation," Opt. Express **25**(24), 29560–29573 (2017).
22. P. S. Nugraha, G. Krizsán, C. Lombosi, L. Pálfalvi, G. Tóth, G. Almási, J. A. Fülöp, and J. Hebling, "Demonstration of a tilted-pulse-front pumped plane-parallel slab terahertz source," Opt. Lett. submitted.
23. M. I. Bakunov and S. B. Bodrov, "Terahertz generation with tilted-front laser pulses in a contact-grating scheme," J. Opt. Soc. Am. B **31**(11), 2549–2557 (2014).
24. K. L. Vodopyanov, "Optical generation of narrow-band terahertz packets in periodically inverted electro-optic crystals: conversion efficiency and optimal laser pulse format," Opt. Express **14**(6), 2263–2276 (2006).
25. X. J. Wu, J. L. Ma, B. L. Zhang, S. S. Chai, Z. J. Fang, C. Y. Xia, D. Y. Kong, J. G. Wang, H. Liu, C. Q. Zhu, X. Wang, C. J. Ruan, and Y. T. Li, "Highly efficient generation of 0.2 mJ terahertz pulses in lithium niobate at room temperature with sub-50 fs chirped Ti:sapphire laser pulses," Opt. Express **26**(6), 7107–7116 (2018).
26. B. C. Stuart, M. D. Feit, A. M. Rubenchik, B. W. Shore, and M. D. Perry, "Laser-Induced Damage in Dielectrics with Nanosecond to Subpicosecond Pulses," Phys. Rev. Lett. **74**(12), 2248–2251 (1995).
27. K. Ravi, W. R. Huang, S. Carbajo, X. Wu, and F. Kärtner, "Limitations to THz generation by optical rectification using tilted pulse fronts," Opt. Express **22**(17), 20239–20251 (2014).
28. L. Pálfalvi, J. Hebling, J. Kuhl, A. Peter, and K. Polgar, "Temperature dependence of the absorption and refraction of Mg-doped congruent and stoichometric LiNbO3 in the THz range," J. Appl. Phys. **97**(12), 123505 (2005).

Optics EXPRESS

29. X. Wu, C. Zhou, W. R. Huang, F. Ahr, and F. X. Kärtner, "Temperature dependent refractive index and absorption coefficient of congruent lithium niobate crystals in the terahertz range," Opt. Express **23**(23), 29729–29737 (2015).